Structural Elements Required for Deamidation of RhoA by Cytotoxic Necrotizing Factor 1†

Lori Buetow‡ and Partho Ghosh*

Department of Chemistry and Biochemistry, University of California at San Diego, La Jolla, California 92093-0314

Received June 30, 2003; Revised Manuscript Received September 8, 2003

ABSTRACT: Cytotoxic necrotizing factor 1 (CNF1), a virulence factor expressed by pathogenic *Escherichia coli*, acts on Rho-GTPases and specifically deamidates a single glutamine residue (Gln-63 in RhoA) required for GTP hydrolysis. This modification constitutively activates the effector binding function of Rho-GTPases and eventually leads to their proteasome-mediated degradation. Previous structural investigation revealed that the CNF1 active site is located in a deep and narrow pocket and that the entrance to this pocket is formed by nine loop segments. We have examined the functional importance of five of these loops (2, 6, 7, 8, and 9) by deleting them individually. We find that deletion of proximally located loops 8 and 9 in the 32 kDa catalytic domain of CNF1 (CNF1-C) nearly or completely abolishes deamidation of RhoA in vitro, identifying a potential Rho-GTPase recognition site. Deletion of loop 7 causes protein folding errors, and deletion of loop 6 has a small effect on deamidation. In contrast, deletion of loop 2 is found to increase deamidation 5−7-fold, implying that this loop rearranges in binding RhoA. None of the loop deletions or wild-type CNF1-C is able to deamidate RhoA containing Asn-63 instead of Gln-63, suggesting that the fit between the toxin and its target is highly precise. In addition, we show that the specificity constant (k_{cat}/K_m) of CNF1-C for RhoA is 825 ± 3 M^{-1} s^{-1}. This modest value is consistent with the confining size of the active site pocket acting to exclude nonspecific targets but also limiting reactivity toward intended targets.

Cytotoxic necrotizing factor 1 (CNF1)[1] is a 114 kDa protein toxin expressed by certain pathogenic strains of *Escherichia coli* (*1*−*3*) and is particularly associated with strains causing urinary tract infections (UTI) or neonatal meningitis. Recent evidence indicates that this protein contributes to virulence by promoting bacterial colonization and invasiveness. In a mouse model of UTI, deletion of CNF1 reduces colonization of kidneys and the bladder by ∼10^6 as compared with an isogenic strain expressing CNF1 (*4*). The CNF1-expressing strain is also seen to cause greater tissue damage in a rat model of acute prostatitis (*5*). Likewise, a CNF1-deficient strain is ∼3-fold less efficient at invading endothelial cells, and its incidence of meningitis in an animal model of disease is ∼3-fold lower (*6*). Invasion of endothelial cells lining the blood−brain barrier is likely to be an important step in meningitis, and similarly, invasion of bladder epithelial cells may be important to uropathogenesis in enabling bacterial migration into deeper tissues during chronic infections (*7*).

These effects of CNF1 arise from its action in the mammalian cytosol following bacterial release, receptor-mediated endocytosis, and translocation out of endocytic vesicles (*8*, *9*). CNF1 targets members of the Rho-GTPase protein family, such as RhoA, Rac1, and Cdc-42 (*10*), which are key regulators of the actin cytoskeleton and also modulate gene transcription (*11*). CNF1 specifically deamidates a single glutamine residue (Gln-63 of RhoA, Gln-61 of Rac1 and Cdc42) that is required for both unassisted and protein-assisted GTP hydrolysis by Rho-GTPases (*10*, *12*−*15*). Deamidation of this glutamine to glutamate constitutively activates the effector binding, GTP-bound state of these proteins and subsequently leads to their degradation through the ubiquitin−proteasome pathway (*7*, *16*). Activation of Rho-GTPases followed by degradation brings about changes in the actin cytoskeleton and membrane structure that lead to bacterial uptake.

The C-terminal third of CNF1 contains its catalytic activity. This portion of the protein is sufficient, when microinjected into target cells, to cause morphological changes characteristic of intoxication by intact CNF1 (*17*). The structure of the C-terminal catalytic domain of CNF1 (CNF1-C, residues 720−1014) has been determined to high resolution (1.83 Å) and provides insight into its enzymatic activity (Figure 1A) (*18*, *19*). CNF1 contains a catalytic triad composed of Cys-866, His-881, and the main chain carbonyl oxygen of Val-833. Cys-866 in its thiolate form carries out nucleophilic attack on the δ-carboxamide of RhoA Gln-63 and is situated at the base of a deep and narrow pocket (Figure 1B). The small size of this pocket is likely to exclude

† This work was supported in part by a W. M. Keck Distinguished Young Scholar Award (P.G.).

* To whom correspondence should be addressed. E-mail: pghosh@ucsd.edu.

‡ Present address: Division of Biological Chemistry and Molecular Microbiology, School of Life Sciences, University of Dundee, Dundee DD1 5EH, U.K.

[1] Abbreviations: βME, β-mercaptoethanol; CD, circular dichroism; CNF1, cytotoxic necrotizing factor 1; CNF1-C, catalytic domain of cytotoxic necrotizing factor 1, residues 720−1014; DTT, dithiothreitol; HRP, horseradish peroxidase; IPTG, isopropyl β-D-thiogalactopyranoside; MBP, maltose binding protein; PVDF, poly(vinylidene fluoride); UTI, urinary tract infection.

10.1021/bi035123l CCC: $25.00
Published on Web 10/16/2003

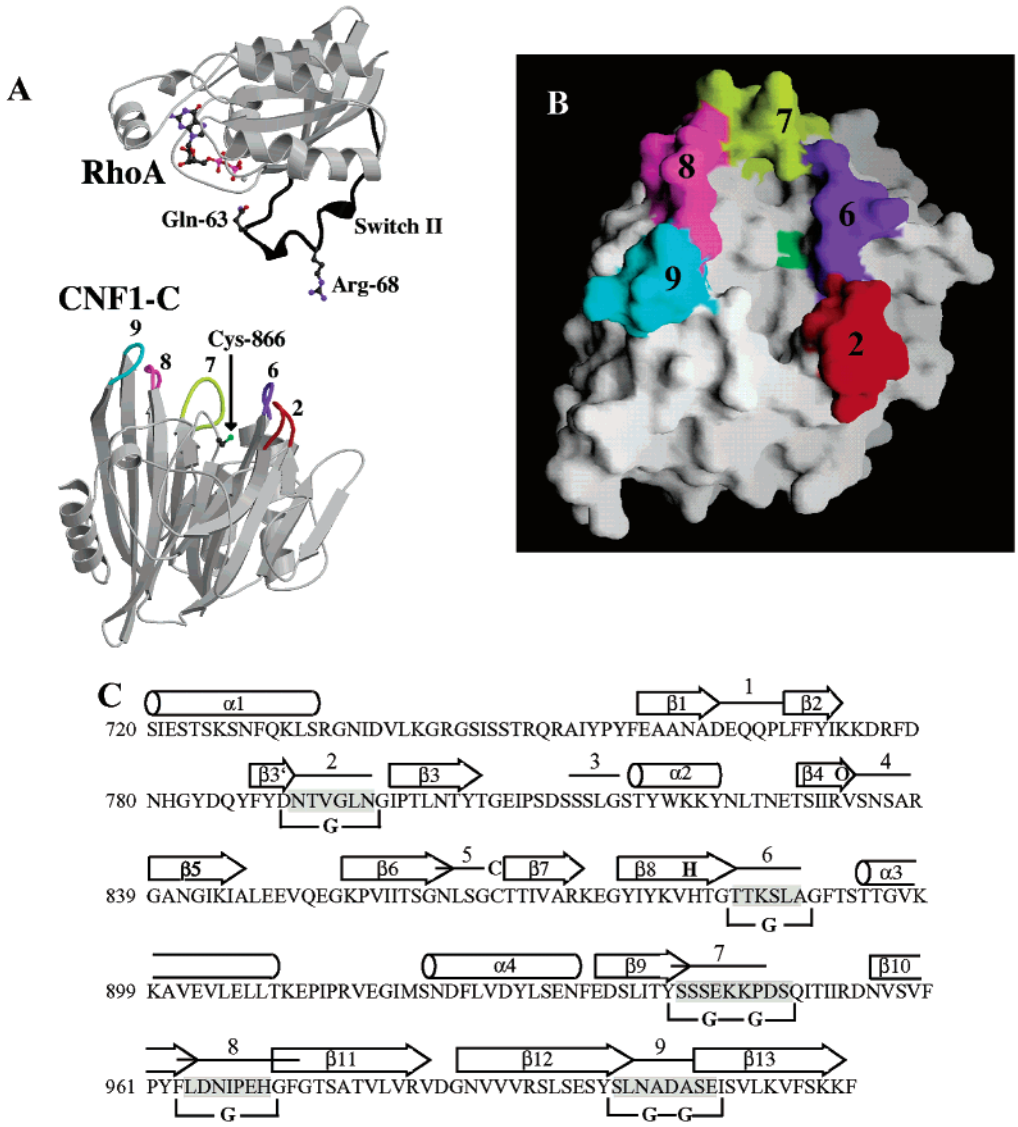

FIGURE 1: CNF1-C and RhoA. (A) Ribbon diagram of RhoA (top) and CNF1-C (bottom). The switch II region of RhoA is in black with Gln-63 and Arg-68 indicated. The loops of CNF1-C targeted for deletion are numbered and colored, and Cys-866 is shown in green. The figure was generated with Molscript (*35*). (B) Molecular surface representation of CNF1-C, with loops targeted for deletion indicated by numbering and coloring (2, red; 6, purple; 7, yellow; 8, magenta; 9, cyan) and with Cys-866 in green. The view is related to the one in panel A by a 60° rotation toward the viewer about a horizontal axis on the page. The figure was generated with Grasp (*36*). (C) Sequence of CNF1-C. Secondary structural elements and catalytic residues are displayed above the sequence. Loops that surround the active site are shown as lines above the sequence and numbered. Residues that are highlighted in gray were deleted and replaced with one or two glycines, as indicated below the sequence.

nonspecific targets from reacting with Cys-866 (*18*) but also indicates that conformational adjustments must occur in accommodating RhoA.

The target glutamine of Rho-GTPases is situated on the switch II region (Figure 1A), which varies in conformation between the GTP- and GDP-bound states. CNF1 acts on both states (*20*), and indeed, a peptide comprising the switch II region (RhoA residues 59−69) suffices as a substrate for deamidation by CNF1 (*21*). Within the switch II region, Arg-68 has been identified by alanine and glycine substitution mutagenesis to be critical for activity by CNF1 (Figure 1A) (*21*, *22*). The only other residue in this region found to affect activity by CNF1 is Leu-72, which when substituted by glutamine disrupts CNF1 activity but when substituted by glycine does not affect activity (*21*, *22*). This indicates that Leu-72 probably comes within contact distance of CNF1. Portions of Rho-GTPases besides the switch II region are likely to be involved in recognition, as the reaction rate on a RhoA switch II peptide (residues 59−78) is 110-fold slower than the reaction rate on intact RhoA (*22*).

How CNF1 recognizes Rho-GTPases, including the important residue Arg-68, is not understood. Previous studies have identified functionally important residues in the active site pocket, such as Cys-866 and His-881, which are strictly required for activity (*17*), and Asn-835 and Ser-864, which affect deamidation activity but are not strictly required (*18*). Cys-866 and His-881 have direct roles in catalysis, and Asn-835 and Ser-864, which bracket Cys-866 in three-dimensional position, are more likely to have indirect roles in catalysis. Initial contacts between CNF1 and Rho-GTPases are likely to occur at the entrance to the active site pocket, which is formed by nine loop regions (Figure 1).

Previously, no appreciable effect on deamidation activity was detected when residues in some of these loop segments

were individually substituted with alanine (*18*). Thus, in this study we used deletion mutagenesis to characterize the functional importance of five of these nine loop segments (2, 6, 7, 8, and 9). Our results highlight the importance of one particular area, formed by the adjacent loops 8 and 9, that is crucial to activity and is likely to be involved in substrate recognition. Deletion of either loop severely impairs or completely abolishes deamidation activity. In contrast, deletion of loop 2 is found to enhance deamidation activity by 5−7-fold as compared to wild-type CNF1-C, indicating that this loop may rearrange upon RhoA binding. We also report that the enzymatic specificity constant (k_{cat}/K_m) of CNF1-C for RhoA is 825 ± 3 M^{-1} s^{-1}, with the K_m for RhoA being at least 250 μM. We discuss the implications of our results for CNF1 activity within mammalian cells.

EXPERIMENTAL PROCEDURES

Expression and Mutagenesis. CNF1-C and mutants of CNF1-C were expressed as previously described (*18*), except that pET28b was used and a C-terminal histidine tag was included. RhoA (residues 2−193, containing F25N) was expressed as a fusion to maltose binding protein (MBP) using pETMALc-H (*23*). Mutagenesis was carried out using the polymerase chain reaction and strand overlap extension (*24*), and DNA sequences of all constructs were verified. Protein expression was induced at midlogarithmic growth of *E. coli* BL21(DE3) with 0.5 mM isopropyl β-D-thiogalactopyranoside (IPTG) (CNF1-C constructs) or 0.1 mM IPTG (RhoA constructs), and bacteria were grown at 25 °C for 4−6 h and harvested by centrifugation (10500*g*, 5 min).

CNF1-C Purification. Bacteria were lysed in 500 mM NaCl, 50 mM sodium phosphate buffer, pH 8, 15 mM imidazole, and 2 mM β-mercaptoethanol (βME) using two to three passes through a French press (Spectronic Unicam, 40K cell). Proteins were purified by nickel chelation (Poros MC/M, Applied Biosystems) followed by size exclusion chromatography (Superdex 75, Amersham Pharmacia). For CNF1-C Δ8 and Δ9, anion-exchange chromatography (Poros 20 HQ/M, Applied Biosystems) was used instead of size exclusion chromatography. Purified proteins were dialyzed in 150 mM NaCl, 20 mM Tris-HCl, pH 8, and 2 mM dithiothreitol (DTT) and stored as snap-frozen aliquots at −80 °C. Protein concentrations were determined using an ϵ_{280} (calculated) of 24890 M^{-1} cm^{-1}.

RhoA Purification. Cells were lysed, as described above, in 500 mM NaCl, 20 mM HEPES, pH 7.5, 5 mM $MgCl_2$, 15 mM imidazole, and 2 mM βME. MBP-RhoA was purified by nickel chelation chromatography (Poros MC/M, Applied Biosystems) and dialyzed in 150 mM NaCl, 20 mM HEPES, pH 7.5, 5 mM $MgCl_2$, and 2 mM βME. Thrombin (Sigma) was used to cleave MBP-RhoA at a 1500:1 mass ratio (substrate:protease) for ~6 h at 25 °C. MBP and uncleaved MBP-RhoA were removed using a second nickel chelation chromatography step, and RhoA was purified further by size exclusion chromatography (Superdex 75, Amersham Pharmacia). For RhoA Q63E and RhoA Q63N, additional purification by anion-exchange chromatography (Poros 20 HQ/M) preceded size exclusion chromatography. Proteins were dialyzed in 150 mM NaCl, 20 mM Tris-HCl, pH 8, and 2 mM DTT and stored as snap-frozen aliquots at −80 °C. Protein concentrations were determined using an ϵ_{280} (calculated, including one guanine nucleotide per RhoA) of 25480 M^{-1} cm^{-1}.

Refolding. The Δ8 mutant protein was refolded from inclusion bodies, which were prepared as previously described with some modifications (*25*). After bacterial cell lysis, cell pellets were suspended and pelleted four times from 50 mM Tris-HCl, pH 8, 0.5% (v/v) Triton X-100, 100 mM NaCl, 1 mM EDTA, 0.1% sodium azide, and 10 mM DTT. Pellets were then suspended and pelleted once from 50 mM Tris-HCl, pH 8, 1 M NaCl, 1 mM EDTA, 0.1% sodium azide, and 10 mM DTT and once from 50 mM Tris-HCl, pH 8, 2 M urea, 1 mM EDTA, 0.1% sodium azide, and 10 mM DTT. Pellets were solubilized in 50 mM Tris-HCl, pH 8, 6 M guanidine hydrochloride, 100 mM DTT, and 0.5 mM EDTA. Proteins were refolded by dialysis at a concentration of 1 μM (in 150 mM NaCl, 50 mM Tris-HCl, pH 8, 1 M L-arginine hydrochloride, pH 8, 1 mM DTT, and 0.5 mM EDTA) at 25 °C for ~30 h and dialyzed in 100 mM NaF, 10 mM Tris-HCl, pH 8, and 0.1 mM DTT (thermal stability assays) or in 150 mM NaCl, 20 mM Tris-HCl, pH 8, and 2 mM DTT (activity assays). As a control, wild-type CNF1-C was denatured in 6 M guanidine hydrochloride, 50 mM Tris-HCl, pH 8, 100 mM DTT, and 0.5 mM EDTA, refolded similarly, and assayed for activity.

Thermal Stability Assays. Wild-type CNF1-C, Δ2, Δ6, Δ8 (refolded), and Δ9 at 2−3 μM in 100 mM NaF, 10 mM Tris-HCl, pH 8, and 0.1 mM DTT were heated from 4 to 52 °C (in 1 °C steps), and the content of secondary structure was followed by the circular dichroism signal at a wavelength of 216 nm (AVIV 62DS spectrapolarimeter). Samples were equilibrated for 30 s at each temperature, and signals were collected over a 5 s time period and averaged. The average molar ellipticity per residue was calculated from duplicate experiments and normalized.

Gel Activity Assays. RhoA or RhoA Q63N at 10 μM was incubated with 200 nM wild-type CNF1-C, Δ2, Δ6, Δ8, Δ9, S864A CNF1-C, or N835A CNF1-C at 25 or 37 °C in assay buffer (150 mM NaCl, 20 mM Tris-HCl, pH 8, 1 mM $MgCl_2$, 1 mM DTT, and 100 μM GDP). Incubations were for up to 2 h for RhoA or 3 h for RhoA Q63N. Samples were separated on denaturing isoelectric focusing (*26*) or 12% SDS−PAGE−urea (1 M) gels (*18*) and stained with Coomassie Blue.

Western Blots. Samples were separated on 12% SDS−PAGE and transferred, following a 30 min incubation in transfer buffer (25 mM Tris-HCl, 192 mM glycine, and 20% methanol), to a poly(vinylidene fluoride) (PVDF) membrane (Osmonics). The blot was incubated in blocking buffer (5% nonfat milk and 1% casein in 150 mM NaCl and 10 mM Tris-HCl, pH 7.5) for 12 h and washed in TBS (150 mM NaCl and 10 mM Tris-HCl, pH 7.5). The blot was then incubated for 2 h in a 1:2500 dilution of rabbit anti-RhoA Q63E antibody (gift from Y. Horiguchi), washed in TBS-T (500 mM NaCl, 20 mM Tris-HCl, pH 7.5, 0.05% Tween 20, and 0.2% Triton X-100), incubated for 1.5 h in a 1:2000 dilution of goat anti-rabbit IgG−horseradish peroxidase (HRP) conjugate (Santa Cruz), and washed again in TBS-T. The blot was visualized on film using ECL Plus (Amersham Pharmacia). All incubations were carried out at 25 °C with shaking.

Standard ELISA Curve. Microtiter plates (Pierce EIA Reacti-Bind plates) were incubated for 2 h with mixtures of

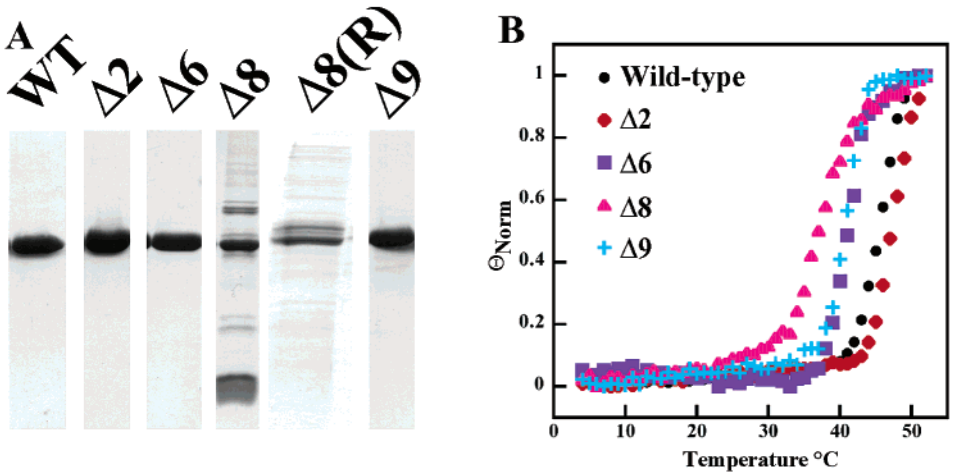

FIGURE 2: Purity and stability of CNF1-C mutants. (A) Purity of proteins used in assays, as visualized by SDS−PAGE and Coomassie Blue staining. Δ8(R) denotes refolded Δ8 protein. (B) Normalized molar ellipticity as a function of temperature (°C) of wild-type (black circles), Δ2 (red tilted squares), Δ6 (purple squares), Δ8 (magenta triangles), and Δ9 (cyan crosses) CNF1-C. Unfolding was measured by CD over a temperature range of 4−52 °C at 216 nm. The average of two separate runs is shown.

RhoA Gln-63 and RhoA Glu-63 (100 μL/well in triplicate), washed with PBS, and incubated for 12 h in blocking buffer (5% nonfat milk, 1% casein, and 0.05% Tween 20 in PBS, 300 μL/well). Thirty-one different mixtures of RhoA Gln-63 and RhoA Glu-63 were made in 150 mM NaCl, 20 mM Tris-HCl, pH 8, 1 mM $MgCl_2$, 100 μM GDP, and 50 mM iodoacetamide, with each sample containing 500 nM total RhoA (sum of RhoA Gln-63 and RhoA Glu-63). The amount of RhoA Glu-63 ranged from 0.01 to 100 nM. Plates were washed in PBS-T (0.05% Tween 20 in PBS), incubated for 2 h in a 1:8000 dilution of anti-RhoA Glu-63 (100 μL/well), washed in PBS-T, and incubated for 1.5 h in a 1:1000 dilution of goat anti-rabbit IgG−HRP conjugate (100 μL/well) (Kirkegaard and Perry Laboratories). Plates were then washed in PBS-T, followed by a final wash in PBS, and incubated with 1-Step Turbo TMB-ELISA (100 μL/well, Pierce) for 30 min. The colorimetric reaction was stopped by the addition of 100 μL of 1.8 M H_2SO_4. The plate was read using a Molecular Devices Spectramax 350PC plate reader at a wavelength of 450 nM, and data were fit with a four-parameter logistic fit (SOFTmax Pro). All incubations were done at 25 °C with agitation.

Initial Rate Studies. RhoA (100, 200, 300, 400, or 500 μM) was reacted with wild-type CNF1-C (54.5 nM) or CNF1-C Δ2 (27.5 nM) in assay buffer as described above. At each RhoA concentration, five to eight selected time points were taken for quantification of RhoA Glu-63 by ELISA. Aliquots of 2 μL of the reactions were removed, and the reaction was stopped by dilution into 198 μL of activity buffer containing 50 mM iodoacetamide. Samples were then diluted in the same buffer so that total RhoA was 500 nM, and 100 μL of this was placed into microtiter plates in triplicate. Each plate also contained six standards (in triplicate), with standards containing 500 nM total RhoA (Gln-63 and Glu-63) and ranging in RhoA Glu-63 from 10 to 35 nM (2−7% RhoA Glu-63). Initial rate determinations were repeated three to nine times at each RhoA concentration. Initial rates (v_0) were determined from the slope of the time course of reaction using a linear fit (and imposing the condition that no product is present at the start of the experiment), and a standard error in the slope (i.e., initial rate) was determined (Kaleidagraph, Synergy Software).

Enzymatic Constants. Weighted linear or Michaelis−Menten fits were carried out in determining K_m/k_{cat} from plots of initial rates, with the standard error in initial rates being used for weighting (Kaleidagraph, Synergy Software). Errors reported for enzymatic constants reflect the standard error of the parameter in fitting. Errors in RhoA concentration reflect the percentage error in measurement of protein concentration. Briefly, a stock RhoA solution was diluted in 6.6 M guanidine hydrochloride and 20 mM potassium phosphate, pH 6.5, and its concentration measured by A_{280}. This was carried out three times to determine an average RhoA concentration and a standard deviation, which was converted to a percentage error.

RESULTS

Loop Deletions. Five of the nine loop segments that form the entrance to the active site pocket of CNF1-C were deleted individually (Figure 1, loops 2, 6, 7, 8, and 9). These loops form connections between antiparallel β-strands, except for loop 7, which forms a connection between parallel β-strands, and loop 6, which connects a β-strand to an α-helix. Deletions were designed on the basis of a study showing that β-hairpins are most often connected by diglycine loops (*27*). Accordingly, the 5−10 residues in each of the five CNF1-C loops were substituted by one or two glycines (Figure 1C). For loops 2, 6, and 8, a single glycine was used for substitution because the sequence of CNF1 provides the second glycine predicted to complete the turn. Molecular modeling is consistent with these changes resulting in removal of the targeted loops but not altering the secondary structural elements that they otherwise connect.

The loop deletion constructs were expressed in *E. coli* and assayed for solubility. Deletion of loop 7 (Δ7) proved detrimental, as the mutant protein was entirely insoluble (data not shown). The four other loop deletions resulted in proteins with partial solubility, similar in the case of Δ2, Δ6, and Δ9 to the partial solubility observed for wild-type CNF1-C and in the case of Δ8 lower than that observed for wild-type CNF1-C (*19*). The solubly expressed portions of Δ2, Δ6, Δ8, and Δ9 were purified (Figure 2A). Protein refolding was pursued for Δ7 and Δ8, since Δ7 was entirely insoluble

and the solubly expressed fraction of Δ8 was difficult to purify to homogeneity (Figure 2A). A condition that promotes refolding of wild-type CNF1-C was first identified, and refolded wild-type CNF1-C was verified to have RhoA deamidase activity (data not shown). Refolding of Δ7 under the same conditions was tried but proved to be refractory, with the protein remaining insoluble. Refolding of Δ8 resulted in soluble protein, and refolded Δ8 was amenable to greater purification than solubly expressed Δ8 (Figure 2A).

Stability of Loop Deletion Mutants. Purified Δ2, Δ6, Δ8, and Δ9 mutant proteins were next tested for stability. Refolded Δ8 (as opposed to unrefolded Δ8) was used in this determination due to its slightly greater purity. Proteins were thermally denatured, and the content of secondary structure was followed using the circular dichroism signal at a wavelength of 216 nm (Figure 2B). Wild-type and loop deletion mutants of CNF1-C each exhibited a single, cooperative unfolding transition. Since denaturation proved to be irreversible (data not shown), we report the temperature to which each protein is stable rather than the melting temperature. While wild-type CNF1-C is stable to ~42 °C, the Δ6 and Δ9 mutant proteins are somewhat destabilized (stable to ~37 °C) and the Δ2 mutant is slightly more stable (to ~42.5 °C). The Δ8 mutant protein is the least stable, although it does not begin denaturing until ~33 °C. The great majority of each of these proteins is stable at 25 °C, and therefore this temperature was chosen for in vitro deamidation assays.

Qualitative Deamidation Assay. The ability of the Δ2, Δ6, Δ8, and Δ9 loop deletion mutants to deamidate RhoA in vitro was assayed qualitatively at 25 °C. Deamidation of RhoA Gln-63 to Glu-63 was detected by SDS−urea−PAGE (Figure 3A), taking advantage of the upward mobility shift caused by the modification. Reaction at 25 °C of 10 μM RhoA with 200 nM wild-type CNF1-C results in nearly complete deamidation over the course of 90 min to 2 h. Reaction under the same conditions with the Δ2 mutant protein results in nearly complete deamidation within a shorter time period (30 min), raising the possibility that Δ2 is more active than wild-type CNF1-C. Reaction with the Δ6 mutant results in substrate remaining visible after 2 h, similar to results observed for CNF1-C S864A and CNF1-C N835A, the single-site mutants that have previously been characterized (*18*).

In contrast to the Δ2 and Δ6 mutants that retain activity, the Δ8 and Δ9 mutants are severely compromised in activity. No product formation is observed for Δ8, and only minor product formation is observed for Δ9 (Figure 3A). To assess whether Δ8 has any deamidation activity at all, the formation of RhoA Glu-63 was detected by Western blot using polyclonal antibodies (*28*). As shown in Figure 3B, these antibodies are specific to RhoA Glu-63 and do not recognize unmodified RhoA. Using this more sensitive detection method, we find that RhoA Glu-63 is produced by all mutants except Δ8. The lack of activity in Δ8 was further confirmed by reacting RhoA with this mutant protein for ~20 h at 4 °C. In contrast to the activity displayed by wild-type CNF1-C under these conditions, Δ8 does not yield detectable product as assayed by Western blot (data not shown). Similarly, refolded Δ8 is found to lack deamidation activity in all conditions tested (data not shown). These results identify loop segments 8 and 9, which form one side of the entrance to the active site pocket (Figure 1C), as being crucial to deamidation of RhoA.

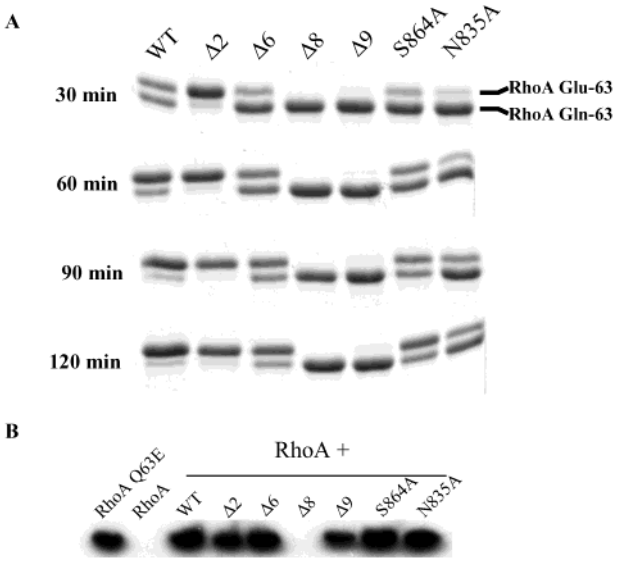

FIGURE 3: Deamidation activity. (A) Deamidation of RhoA by wild-type CNF1-C, Δ2, Δ6, Δ8, Δ9, S864A, or N835A detected by SDS−urea−PAGE (12%, 1 M). RhoA (10 μM) was reacted with wild-type or mutant CNF1-C (200 nM) at 25 °C for the times indicated, and the positions of the substrate (RhoA Gln-63, lower band) and product (RhoA Glu-63, upper band) are indicated at the right in the first panel. (B) Western blot detection using an anti-RhoA Q63E antibody of RhoA reacted with wild-type CNF1-C, Δ2, Δ6, Δ8, Δ9, S864A, or N835A for 90 min under the same conditions as in panel A. Samples were separated on 12% SDS−PAGE, and the first two lanes contain RhoA Q63E and unmodified RhoA as standards.

Steady-State Kinetic Assays. Enzymatic constants for CNF1 action on RhoA are unknown. To measure these, we developed an enzyme-linked immunosorbent assay (ELISA) for quantification of RhoA Glu-63. For this assay, RhoA and other components in the reaction were adhered to a solid substrate, and RhoA Glu-63 was detected using the anti-RhoA Glu-63 polyclonal antibodies described above (*28*). To verify that unmodified RhoA (Gln-63) does not interfere with quantification, a standard curve was constructed from samples containing both unmodified RhoA (Gln-63) and modified RhoA (Glu-63) (Figure 4A). This curve mimics the progress of the reaction. Each sample contains 500 nM total RhoA (sum of unmodified and modified RhoA), but the ratio of unmodified to modified RhoA differs in each sample. The first sample contains 0.002% modified RhoA (0.01 nM), the last sample contains 20% modified RhoA (100 nM), and samples in between contain intermediate percentages of modified RhoA. The standard curve shows that RhoA Glu-63 is detected linearly between 10 nM (in a background of 490 nM unmodified RhoA) and 75 nM (in a background of 425 nM unmodified RhoA) (Figure 4A). This translates to detection of product between 2% to 15% turnover, well within steady-state conditions. The presence of CNF1-C (inhibited with the cysteine-reactive agent iodoacetamide) does not have any effect on the standard curve.

Initial rates of reaction of wild-type CNF1-C with RhoA were then determined at 25 °C using this ELISA. RhoA, at concentrations ranging from 100 to 500 μM, was reacted for varying times with 55 nM CNF1-C, and the amount of RhoA Glu-63 produced was quantified by ELISA after the

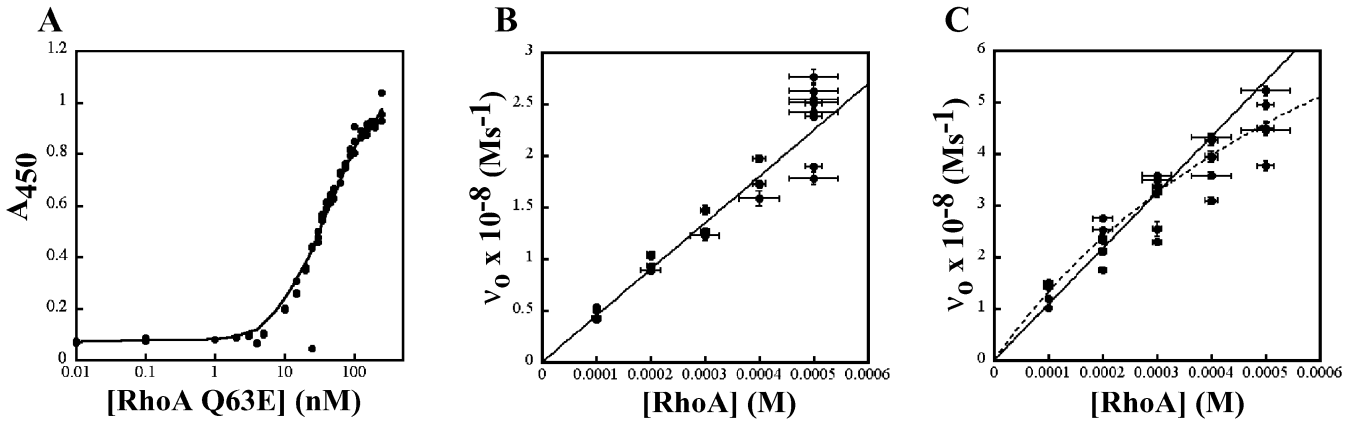

FIGURE 4: Steady-state kinetic determinations. (A) Standard ELISA curve for detection of RhoA Glu-63. Each point contains differing mixtures of RhoA Glu-63 and RhoA Gln-63, with the total RhoA maintained at 500 nM. RhoA Glu-63 was detected by ELISA using rabbit anti-RhoA Q63E polyclonal antibodies and an anti-rabbit IgG−HRP conjugate. Each sample was measured in triplicate. (B and C) Initial rate plots for deamidation of RhoA by (B) wild-type CNF1-C (54.5 nM) and (C) Δ2 (27.5 nM). The solid line corresponds to a linear fit of data, and the dashed line to a Michaelis−Menten fit. Standard errors in v_0 (vertical) and percentage errors in RhoA concentration (horizontal) are shown.

reaction was stopped with iodoacetamide. Initial rates were determined from the linear portion of reaction time courses, which corresponds to a maximum substrate turnover of 10%, and are plotted in Figure 4B. Across the entire range of RhoA concentrations up to 500 μM, no saturation of initial rates is evident, and instead rates are seen to increase linearly. Higher concentrations of RhoA could not be assayed due to the solubility limits in this experiment. These results reveal that the specificity constant, k_{cat}/K_m, for CNF1-C deamidation of RhoA is 825 ± 3 M^{-1} s^{-1}. Due to the lack of saturation, these data do not allow separate determinations of K_m and k_{cat} to be made. However, these results do permit estimations on the lower limit of these enzymatic constants. These data are consistent with K_m being greater than 250 μM RhoA (or half of the maximum RhoA concentration tested) and k_{cat} being greater than 0.2 s^{-1}.

Steady-state kinetics for the Δ2 mutant were next examined using the ELISA. Confirming results from SDS−urea−PAGE experiments, initial rate measurements demonstrate that the Δ2 mutant protein is more active than wild-type CNF1-C. In contrast to wild-type CNF1-C, initial rates for Δ2 begin saturating at higher RhoA concentrations. Both linear and Michaelis−Menten fits were carried out with the data, but it should be noted that the Michaelis−Menten fit is only approximate due to the data representing only the initial phase of enzyme saturation. The linear fit gives a k_{cat}/K_m of 3930 ± 121 M^{-1} s^{-1}, and the Michaelis−Menten fit gives a k_{cat}/K_m of 5390 ± 330 M^{-1} s^{-1} (Figure 4C). These results indicate that the Δ2 mutant is approximately 5−7 times more active than wild-type CNF1-C. Furthermore, the Michaelis−Menten fit of Δ2 yields a K_m for RhoA of 810 ± 28 μM and a k_{cat} of 4.36 ± 0.11 s^{-1}.

Variations in RhoA. We next asked whether deletion of these loops would extend the activity of CNF1-C toward an altered RhoA substrate, containing Asn rather than Gln at residue 63. The RhoA Q63N mutant was constructed, expressed, and purified, and deamidation activity at 25 °C on RhoA Asn-63 was followed using a denaturing isoelectric focusing gel (Figure 5). Deamidation by wild-type CNF1-C of RhoA Gln-63 to Glu-63 is seen to result in a downward mobility shift due to the gain of a single negative charge. In contrast, when RhoA Asn-63 is incubated with CNF1-C, no

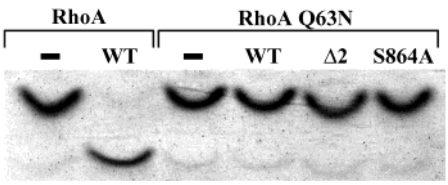

FIGURE 5: RhoA Q63N does not react with wild-type or mutant CNF1-C. Denaturing isoelectric focusing gel of RhoA (10 μM) reacted with wild-type CNF1-C (200 nM) and RhoA Q63N (10 μM) reacted with wild-type CNF1-C, Δ2, and S864A CNF1-C (200 nM) for 3 h at 25 °C.

downward shift is evident. This indicates that RhoA Asn-63 is not deamidated to RhoA Asp-63 by wild-type CNF1-C. Similarly, the Δ2 loop deletion mutant and the single-site mutant CNF1-C S864A are seen to lack deamidation activity on RhoA Asn-63. Additionally, none of the other loop deletions (Δ6, Δ8, and Δ9) or the single-site mutant CNF1-C N835A exhibits deamidation activity on RhoA Asn-63 and neither does reaction with wild-type CNF1-C at the higher temperature of 37 °C (data not shown). These results are consistent with wild-type and mutant forms of CNF1-C interacting with RhoA in a highly precise way, such that reduction in the length of the substrate by a single methyl group compromises catalysis.

DISCUSSION

We undertook a mutagenesis approach to identify regions of the catalytic domain of CNF1 (CNF1-C) that are important for function. Several studies have revealed the functional importance of active site residues and those proximal to the active site (*17*, *18*), but little is known of other regions. We assessed the importance of loops that form the edges of the active site pocket and are likely to be initial sites of contact with Rho-GTPases. These loops are distant from the active site cysteine (generally, >10 Å), suggesting that their potential function is more likely to be in substrate discrimination rather than chemical catalysis. Previously, a number of single-site mutations in these loop regions (L974P in loop 2, E943A in loop 7, N966A in loop 8) were found to yield little or no effect on deamidation (*18*), and therefore, entire loops were deleted in this study.

We deleted five (2, 6, 7, 8, and 9) of the nine loops surrounding the active site (Figure 1), and while one of these deletions resulted in protein folding errors (Δ7), the others yielded soluble proteins. Two of the loop deletion mutants resulted in proteins with severely decreased or absent in vitro RhoA deamidation activities as assayed at 25 °C, a temperature at which a substantial fraction of all tested mutants are folded. The most severely affected deletion mutant in terms of deamidation activity is Δ8. Approximately 90% of Δ8 is folded at 25 °C and ∼98% at 4 °C, but this deletion mutant is found to entirely lack deamidation activity at either temperature. These conclusions are valid for both the solubly expressed portion of Δ8, which is not homogeneous in its purified form, and for refolded Δ8, which is more homogeneous in its purified form. The most likely explanation for Δ8 lacking deamidation activity is loss of catalytic function, as opposed to other explanations such as the presence of an impurity that inhibits deamidation or a defect in stability. It seems highly unlikely that the lack of deamidation activity of solubly expressed Δ8 can be explained by the occurrence of an inhibitor of deamidation in this inhomogeneous preparation, as unpurified bacterial lysates containing wild-type CNF1-C were found to have RhoA deamidation activity (data not shown). And concerns about the success of refolding Δ8 are assuaged by the observations that refolded Δ8 consists of cooperatively folded protein (Figure 2) and that refolding of denatured, wild-type CNF1-C using the same conditions results in functional protein. Likewise, loss of catalytic function is the most likely explanation for the barely detectable deamidation activity of the Δ9 mutant. The Δ9 mutant protein is expressed at a level of solubility similar to that of wild-type CNF1-C and was purified to a high level of homogeneity. Additionally, the ∼94% of Δ9 folded at 25 °C is equivalent to the percentage of wild-type CNF1-C folded at this temperature. Therefore, the compromised deamidation activities of both Δ8 and Δ9 mutant proteins are most consistent with these loops having key roles in function. Interestingly, loops 8 and 9 are positioned adjacent to one another on one side of the binding pocket (Figure 1). Their location and critical role in deamidation strongly suggest that these loops function as a Rho-GTPase recognition site, but it should be kept in mind that a function in chemical catalysis cannot be formally excluded at this time. Single-site substitutions will be required to map these regions in greater detail. We note that loops 8 and 9 both have several acidic residues that are potential sites of contact with Arg-68 of RhoA.

In striking contrast to results with Δ8 and Δ9, deletion of loop 2 is found to increase deamidation activity 5−7-fold as compared with wild-type CNF1-C. This suggests that loop 2 inhibits substrate binding and needs to rearrange in accommodating RhoA, consistent with molecular modeling studies that indicate a requirement for conformational adjustments (*18*). The Δ2 mutant may be useful in studying direct interactions between CNF1-C and RhoA.

None of the deletion mutants or wild-type CNF1-C is able to deamidate RhoA containing an asparagine rather than glutamine at position 63. This mutation reduces the length of the substrate by one methyl carbon. Resistance to deamidation of this shortened substrate implies that the steric fit between RhoA and CNF1-C is highly precise. This fit appears not to be altered in any of the CNF1-C mutants. These results are also consistent with an experiment examining whether Cys-866 of CNF1-C is capable of forming a disulfide bond with RhoA containing a cysteine at position 63. We constructed, expressed, and purified RhoA Q63C but were unable by nonreducing SDS−PAGE to find evidence for disulfide bond formation with CNF1-C (L. Buetow and P. Ghosh, unpublished results). The cysteine suflhydryl is at the γ-position of the side chain in contrast to the δ-carboxamide of glutamine and, thus, one bond length shorter than the natural substrate. Further evidence for a precise conformational fit between CNF1-C and RhoA comes from the finding that RhoA L72G but not RhoA L72Q is capable of being modified by CNF1 (*22*).

We also examined the steady-state kinetics of CNF1-C action on RhoA. The specificity constant (k_{cat}/K_m) of 825 ± 3 M^{-1} s^{-1} for CNF1-C is within the range found for other toxins. While Shiga toxin (activated with urea and DTT) has been estimated to have a much greater specificity constant of $\sim 10^7$ M^{-1} s^{-1} for its ribosomal RNA target (*29*), tetanus toxin has been shown to have a lower specificity constant of ∼300 M^{-1} s^{-1} as a synaptobrevin-specific protease (*30*). Diphtheria toxin (DT), a highly potent toxin able to cause cell death through the action of a single molecule (*31*), serves as a useful point of comparison. DT binds to its host cell receptor with high affinity (K_d of 7 pM) (*32*) and acts within the host cytosol with a specificity constant of $\sim 10^6$ M^{-1} s^{-1} (*33*). CNF1, like DT, has high affinity for its receptor (K_d of 20 pM) (*8*) but a specificity constant that is ∼1000-fold lower. This difference stems in part from differences in K_m, which for ADP-ribosylation of EF-2 by DT is 0.9 μM (*33*). In contrast, the lower limit of K_m established for CNF1 is 250 μM RhoA. This probably reflects the abundant nature of the substrate for CNF1, with the total cellular concentration of Rho-GTPases estimated at ∼2−5 μM (*34*).

The high K_m of CNF1 for RhoA may also reflect the cost of achieving high target specificity. Isolation of the active site in a deep and narrow pocket serves to exclude nonspecific targets, allowing CNF1 to work in a circumscribed as opposed to promiscuous manner in host cells and curtailing its activity to its intended substrate. At the same time, isolation of the active site also probably limits affinity and reaction rates for Rho-GTPases. The balance achieved by CNF1 between action on its intended target and exclusion of unintended targets appears to be effective in bringing about precise changes in host cell behavior beneficial to pathogenic *E. coli*.

ACKNOWLEDGMENT

We thank Dr. Elizabeth Komives for assistance in interpretation of enzymatic data, Dr. Y. Horiguchi for anti-RhoA Q63E antibody, and members of the laboratory for technical assistance and discussion.

REFERENCES

1. De Rycke, J., Phan-Thanh, L., and Bernard, S. (1989) Immunochemical identification and biological characterization of cytotoxic necrotizing factor from *Escherichia coli*, *J. Clin. Microbiol. 27*, 983−988.
2. Boquet, P. (2001) The cytotoxic necrotizing factor 1 (CNF1) from *Escherichia coli*, *Toxicon 39*, 1673−1680.
3. Horiguchi, Y. (2001) *Escherichia coli* cytotoxic necrotizing factors and Bordetella dermonecrotic toxin: the dermonecrosis-inducing toxins activating Rho small GTPases, *Toxicon 39*, 1619−1627.

4. Rippere-Lampe, K. E., O'Brien, A. D., Conran, R., and Lockman, H. A. (2001) Mutation of the gene encoding cytotoxic necrotizing factor type 1 (cnf1) attenuates the virulence of uropathogenic *Escherichia coli*, *Infect. Immun. 69*, 3954−3964.
5. Rippere-Lampe, K. E., Lang, M., Ceri, H., Olson, M., Lockman, H. A., and O'Brien, A. D. (2001) Cytotoxic necrotizing factor type 1-positive *Escherichia coli* causes increased inflammation and tissue damage to the prostate in a rat prostatitis model, *Infect. Immun. 69*, 6515−6519.
6. Khan, N. A., Wang, Y., Kim, K. J., Chung, J. W., Wass, C. A., and Kim, K. S. (2002) Cytotoxic necrotizing factor-1 contributes to *Escherichia coli* K1 invasion of the central nervous system, *J. Biol. Chem. 277*, 15607−15612.
7. Doye, A., Mettouchi, A., Bossis, G., Clement, R., Buisson-Touati, C., Flatau, G., Gagnoux, L., Piechaczyk, M., Boquet, P., and Lemichez, E. (2002) CNF1 exploits the ubiquitin-proteasome machinery to restrict Rho GTPase activation for bacterial host cell invasion, *Cell 111*, 553−564.
8. Contamin, S., Galmiche, A., Doye, A., Flatau, G., Benmerah, A., and Boquet, P. (2000) The p21 Rho-activating toxin cytotoxic necrotizing factor 1 is endocytosed by a clathrin-independent mechanism and enters the cytosol by an acidic-dependent membrane translocation step, *Mol. Biol. Cell 11*, 1775−1787.
9. Pei, S., Doye, A., and Boquet, P. (2001) Mutation of specific acidic residues of the CNF1 T domain into lysine alters cell membrane translocation of the toxin, *Mol. Microbiol. 41*, 1237−1247.
10. Oswald, E., Sugai, M., Labigne, A., Wu, H. C., Fiorentini, C., Boquet, P., and O'Brien, A. D. (1994) Cytotoxic necrotizing factor type 2 produced by virulent *Escherichia coli* modifies the small GTP-binding proteins Rho involved in assembly of actin stress fibers, *Proc. Natl. Acad. Sci. U.S.A. 91*, 3814−3818.
11. Hall, A. (1998) Rho GTPases and the actin cytoskeleton, *Science 279*, 509−514.
12. Flatau, G., Lemichez, E., Gauthier, M., Chardin, P., Paris, S., Florentini, C., and Boquet, P. (1997) Toxin-induced activation of the G protein p21 Rho by deamidation of glutamine, *Nature 387*, 729−733.
13. Schmidt, G., Sehr, P., Wilm, M., Selzer, J., Mann, M., and Aktories, K. (1997) Gln 63 of Rho is deamidated by *Escherichia coli* cytotoxic necrotizing factor-1, *Nature 387*, 725−729.
14. Fiorentini, C., Fabbri, A., Flatau, G., Donelli, G., Matarrese, P., Lemichez, E., Falzano, L., and Boquet, P. (1997) *Escherichia coli* cytotoxic necrotizing factor 1 (CNF1), a toxin that activates the Rho GTPase, *J. Biol. Chem. 272*, 19532−19537.
15. Lerm, M., Selzer, J., Hoffmeyer, A., Rapp, U. R., Aktories, K., and Schmidt, G. (1999) Deamidation of Cdc42 and Rac by *Escherichia coli* cytotoxic necrotizing factor 1: activation of c-Jun N-terminal kinase in HeLa cells, *Infect. Immun. 67*, 496−503.
16. Lerm, M., Pop, M., Fritz, G., Aktories, K., and Schmidt, G. (2002) Proteasomal degradation of cytotoxic necrotizing factor 1-activated rac, *Infect. Immun. 70*, 4053−4058.
17. Schmidt, G., Selzer, J., Lerm, M., and Aktories, K. (1998) The Rho-deamidating cytotoxic necrotizing factor 1 from *Escherichia coli* possesses transglutaminase activity. Cysteine 866 and histidine 881 are essential for enzyme activity, *J. Biol. Chem. 273*, 13669−13674.
18. Buetow, L., Flatau, G., Chiu, K., Boquet, P., and Ghosh, P. (2001) The structure of the Rho-activating domain of *E. coli* cytotoxic necrotizing factor type 1, *Nat. Struct. Biol. 8*, 584−588.
19. Buetow, L., Flatau, G., Chiu, K., Boquet, P., and Ghosh, P. (2002) Strategies for the structural determination of the catalytic domain of *Escherichia coli* cytotoxic necrotizing factor 1, *Acta Crystallogr. D58*, 366−369.
20. Schmidt, G., Goehring, U. M., Schirmer, J., Lerm, M., and Aktories, K. (1999) Identification of the C-terminal part of Bordetella dermonecrotic toxin as a transglutaminase for rho GTPases, *J. Biol. Chem. 274*, 31875−31881.
21. Flatau, G., Landraud, L., Boquet, P., Bruzzone, M., and Munro, P. (2000) Deamidation of RhoA glutamine 63 by the *Escherichia coli* CNF1 toxin requires a short sequence of the GTPase switch 2 domain, *Biochem. Biophys. Res. Commun. 267*, 588−592.
22. Lerm, M., Schmidt, G., Goehring, U. M., Schirmer, J., and Aktories, K. (1999) Identification of the region of rho involved in substrate recognition by *Escherichia coli* cytotoxic necrotizing factor 1 (CNF1), *J. Biol. Chem. 274*, 28999−29004.
23. Pryor, K. D., and Leiting, B. (1997) High-level expression of soluble protein in *Escherichia coli* using a His6-tag and maltose-binding-protein double-affinity fusion system, *Protein Expression Purif. 10*, 309−319.
24. Higuchi, R., Krummel, B., and Saiki, R. K. (1988) A general method of in vitro preparation and specific mutagenesis of DNA fragments: study of protein and DNA interactions, *Nucleic Acids Res. 16*, 7351−7367.
25. Garboczi, D. N., Utz, U., Ghosh, P., Seth, A., Kim, J., VanTienhoven, E. A., Biddison, W. E., and Wiley, D. C. (1996) Assembly, specific binding, and crystallization of a human TCR-alphabeta with an antigenic Tax peptide from human T lymphotropic virus type 1 and the class I MHC molecule HLA-A2, *J. Immunol. 157*, 5403−5410.
26. Ausubel, F. M., Brent, R., Kingston, R. E., Moore, D. D., Seidman, J. G., and Struhl, K., Eds. (1987) *Current Protocols in Molecular Biology*, Wiley, New York.
27. Gunasekaran, K., Ramakrishnan, C., and Balaram, P. (1997) Beta-hairpins in proteins revisited: lessons for de novo design, *Protein Eng. 10*, 1131−1141.
28. Sugai, M., Hatazaki, K., Mogami, A., Ohta, H., Peres, S. Y., Herault, F., Horiguchi, Y., Masuda, M., Ueno, Y., Komatsuzawa, H., Suginaka, H., and Oswald, E. (1999) Cytotoxic necrotizing factor type 2 produced by pathogenic *Escherichia coli* deamidates a gln residue in the conserved G-3 domain of the rho family and preferentially inhibits the GTPase activity of RhoA and rac1, *Infect. Immun. 67*, 6550−6557.
29. Brigotti, M., Carnicelli, D., Alvergna, P., Mazzaracchio, R., Sperti, S., and Montanaro, L. (1997) The RNA-N-glycosidase activity of Shiga-like toxin I: kinetic parameters of the native and activated toxin, *Toxicon 35*, 1431−1437.
30. Soleilhac, J. M., Cornille, F., Martin, L., Lenoir, C., Fournie-Zaluski, M. C., and Roques, B. P. (1996) A sensitive and rapid fluorescence-based assay for determination of tetanus toxin peptidase activity, *Anal. Biochem. 241*, 120−127.
31. Yamaizumi, M., Mekada, E., Uchida, T., and Okada, Y. (1978) One molecule of diphtheria toxin fragment A introduced into a cell can kill the cell, *Cell 15*, 245−250.
32. Cha, J. H., Brooke, J. S., Chang, M. Y., and Eidels, L. (2002) Receptor-based antidote for diphtheria, *Infect. Immun. 70*, 2344−2350.
33. Wilson, B. A., Reich, K. A., Weinstein, B. R., and Collier, R. J. (1990) Active-site mutations of diphtheria toxin: effects of replacing glutamic acid-148 with aspartic acid, glutamine, or serine, *Biochemistry 29*, 8643−8651.
34. Michaelson, D., Silletti, J., Murphy, G., D'Eustachio, P., Rush, M., and Philips, M. R. (2001) Differential localization of Rho GTPases in live cells: regulation by hypervariable regions and RhoGDI binding, *J. Cell Biol. 152*, 111−126.
35. Kraulis, P. (1991) MOLSCRIPT: a program to produce both detailed and schematic plots of proteins, *J. Appl. Crystallogr. 24*, 946−950.
36. Nicholls, A., Sharp, K., and Honig, B. (1991) Protein folding and association: insights from the interfacial and thermodynamic properties of hydrocarbons, *Proteins 11*, 281−296.

BI035123L